SIMULATION OF INDETERMINATE MULTI-POINT IMPACT AND CONTACT WITH FRICTION

by

ADRIAN RODRIGUEZ

Presented to the Faculty of the Graduate School of
The University of Texas at Arlington in Partial Fulfillment
of the Requirements
for the Degree of

MASTER OF SCIENCE IN MECHANICAL ENGINEERING

THE UNIVERSITY OF TEXAS AT ARLINGTON

December 2010

To my better half who has stood by my side with unvalued support,

to my siblings who set the example with their success, and

to my parents who guided and raised me to make me who I am.

ACKNOWLEDGEMENTS

I would like to thank my supervising professor Dr. Alan Bowling for constantly pushing me to never give up. His encouraging words and invaluable advice helped guide me through the course of my research. I would like to thank my academic advisor Dr. Albert Tong and associate professor Dr. Panos Shiakolas for their continuous support and academic guidance. I would also like to thank Dr. Kamesh Subbarao and Dr. Daejong Kim for their interest in my research and for serving in my thesis committee.

I wish to thank all my teachers through middle and high school and the Upward Bound Math and Science program for establishing the foundation of my education. I would also like to thank Dr. John Haglund, Dr. Desiderio Kovar, Dr. Raul Longoria, Dr. Eric Fahrenthold, and the Intellectual Entrepreneurship program at The University of Texas at Austin who inspired and supported my efforts to pursue graduate studies. I am grateful to all the co-workers during my higher education, especially Ms. Minnie Russell, Ms. Lori Cantu, and Mr. Robert Wheeler III, J.D. for their relentless support.

Finally, I would like to express my deepest gratitude to all my family and friends who helped me throughout the years. I sincerely appreciate the caring support and patience from my better half. I am blessed to have siblings who established the path for pursuing higher education and set the example. I am also extremely grateful to my mother and father for their constant encouragement and sacrifice.

November 23, 2010

ABSTRACT

SIMULATION OF INDETERMINATE MULTI-POINT
IMPACT AND CONTACT WITH FRICTION

ADRIAN RODRIGUEZ, M.S.

The University of Texas at Arlington, 2010

Supervising Professor: Alan Bowling

This work presents a method for determining the post-impact behavior of a rigid-body undergoing simultaneous, multiple impacts with friction. A discrete algebraic model is used with an event-driven function which finds impact events. In this work, the indeterminate nature of the equations of motion encountered at impact are examined. A velocity constraint is developed based on the rigid-body assumption to address the equations and an impact law is used to determine the impulsive forces. The slip-state of each contact point is then determined and appropriate methods are used to resolve the post-impact velocities. Friction is treated as a complementarity problem and a set complementarity conditions are formulated using Coulomb's friction law. Additional constraints are composed in terms of a dissipation principle to yield a solution for the post-impact tangential velocities. These works will be applied to a simple planar model of a ball which is forced to impact a corner between the ground and a wall. Computer simulations will be presented to demonstrate the post-impact behavior of a rigid-body which experiences simultaneous, multiple impacts with friction.

TABLE OF CONTENTS

Appendix

LIST OF FIGURES

LIST OF TABLES

CHAPTER 1

INTRODUCTION

A vast amount of work has been performed in the simulation of rigid-body impact and contact. The theory governing rigid-body collisions extends to the treatment of impact at multiple points with or without friction at the contact points [1, 2, 3]. Although, very little work has been done on the study of multiple impacts with friction when they occur simultaneously on a rigid-body [1, 4, 5, 6]. The equations of motion result as an indeterminate system of equations in which the number of impact forces are more than the number equations available. These impact forces must be solved in order to determine the slip-state of each contact point. Thus, a method must be utilized to overcome the indeterminacy of the equations of motion and motivate a solution for the impact forces. This will allow for a calculation of the post-impact velocities which dictate the behavior of the system after impact.

1.1 Model Description

A simple planar model of a ball with radius R is considered in this work and is shown in Fig. 1.1. The model contains three degrees of freedom denoted by Q_1, Q_2, and Q_3. The ball's position is indicated by the position vector $\mathbf{P_{NA}}$. The angular rotation of the ball about the $\mathbf{N_3}$ direction is represented by Q_3. At the point of impact, the ball is in simultaneous contact with the ground and the wall. Two force components are present at each contact point which are depicted as F_1, F_2, F_3, and F_4. One force is normal to the surface and the second is tangential to the surface

caused by friction. The angle of impact, θ, with respect to the ground is determined by the velocity components of the ball, $\mathbf{v_A}$, at the instant before impact.

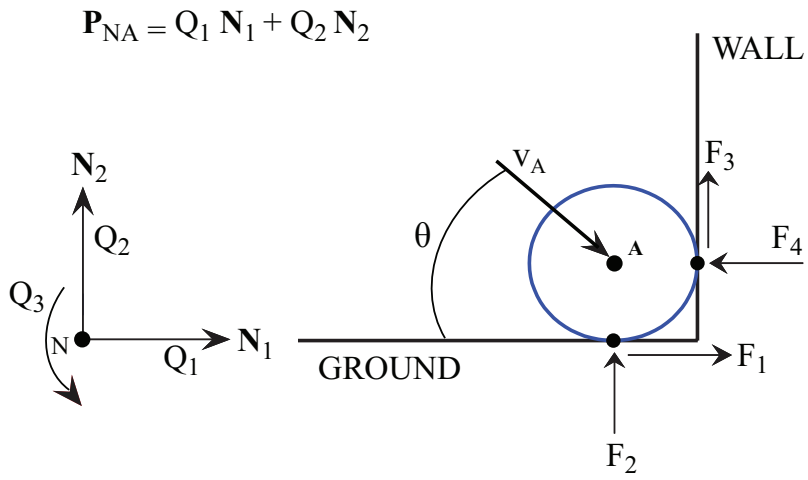

Figure 1.1. Simple Planar Model.

1.2 Methods Used

It is important to know the impulsive forces at impact to evaluate the slip-state of each contact point. Appropriate methods can then be employed to resolve the post-impact velocities. This work presents a unique method to overcome the difficulty of calculating the impulsive forces as a result of the indeterminacy of the equations of motion. Based on the rigid-body assumption, a velocity constraint can be enforced to make the equations of motion determinate. An impact law is developed with the implementation of the velocity constraint to calculate the impulsive forces. Friction at the impact points is treated as a complementarity problem where a set of conditions are formulated using Coulomb's friction law [7]. These conditions along with the known static and dynamic coefficients of friction define the sticking and slipping

regions for the post-impact velocities in the tangential direction. A boundary exists between the stick and slip regions known as the stick-slip transition which introduces a discontinuity when evaluating the slip-state of a contact point. A Karnopp model is adopted to address this discontinuity which helps smooth the transition between the two regions [8]. The conditions introduced by the complementarity problem only define the feasible range of values for the velocities, accelerations, and forces. In order to acheive a solution for the post-impact tangential velocities, additional constraints are needed [9]. Thus, a dissipation principle which minimizes a quantity of interest is formulated to find the minimum feasible solution for the tangential velocities [10, 11, 12]. The major developments made in this work are

- development of a velocity constraint which addresses the indeterminate nature of the equations of motion
- derivation of an impact law with the use of the velocity constraint to determine the impulsive forces
- demonstrate the post-impact dynamic behavior of a system which experiences simultaneous, multi-point impact and contact with friction

The remaining paper will be organized as followed. Background will be presented on the various approaches which have been pursued to analyze the impact problem and the approach considered in this work. The problem statement for this work will be stated and the development of a velocity constraint based on the rigid-body assumption will be given. Next, a brief discussion of the derivation of an impact law which uses the velocity constraint will be presented followed by the theory used to resolve the post-impact velocities of the system. Then, the results of three cases analyzed will be presented. The paper will end with some meaningful conclusions drawn as a result of the cases which were considered.

CHAPTER 2

BACKGROUND

The classical treatment of rigid-body collisions has been extensively studied to model and examine the impact characteristics. The two common approaches used for modeling impact are known as a continuous and discontinuous method. The continuous method does not stop the simulation and treats the impact as part of the dynamics of the system. Hence, the impact forces are added to the dynamic equations of motion at the time of the impact event [13]. The approach used in this work splits the impact event into two regions: before impact and after impact. This approach is referred to as a discontinuous method and it is assumed that the position and orientation of the body does not change during the impact event which occurs over a very short time period [13].

The integrator used in this simulation is Matlab's ode45.m along with an event function that captures when an impact event has occurred. An overview of the numerical integration used to solve the ordinary, differential equations can be found in Appendix A.1. The event function is triggered when a specified position is reached and subsequently terminates the simulation. At that point, the post-impact velocities of the impacting points are calculated algebraically and serve as the initial conditions for when the simulation is restarted. Many different methods have been utilized for determining the post-impact velocities. Some methods use an impulse-momentum balance or discrete method to develop contact and impact laws which examine the impulsive forces [2, 14, 15]. Others have used a direct analysis of energy absorption and restitution but are insufficient alone when friction is involved [16, 17]. In this

work, a discrete algebraic model is used along with the development of an impact law as in [15] which examines the impulses and momenta of the system.

Dynamic modeling of systems involving simultaneous, multiple impacts with friction yield equations of motion which are indeterminate with respect to the impact forces [1, 4, 5, 6]. This indeterminacy is caused by a non-square Jacobian, which is not invertible, and premultiplies the impact forces in the equations of motion. This is problematic because the impact forces are needed to determine the state of sticking or slipping at each impact and contact point. There are methods available which have been used in the literature for addressing this situation. One simple method is to add more degrees-of-freedom to the problem by considering elasticity in the bodies [1]. This is in contrast to rigid-body approaches, which directly consider the properties of the non-square Jacobian.

For example, in [4], the QR factorization is used to determine the impact force components which have the least effect on the system according to the elements in the factorization. The impact forces having the least effect on the dynamics are removed, set equal to zero, in order to allow a solution for the remaining components. In other work, indeterminate contact forces are encountered for robotic manipulators when multiple contact points are involved in grasping an object [5, 6]. These works examine the static friction forces present at the contact points and determine the infeasibility of some solutions. The authors intuitively develop force constraints based on the situation-specific contact geometry of the grasped object to solve the indeterminate equations. These methods are useful and provide a reasonable means to address the indeterminacy of the equations.

In this work, an effort is made to develop a more general approach to addressing contact force indeterminacy than in [5, 6], by using a velocity constraint that is more consistent with the assumptions which form the basis for classical rigid-body impact

analysis, in contrast to [4]. Any point on a rigid-body by definition remains the same distance from all the other points on the body assuming that no deformations take place [18]. Hence, it is possible to formulate a relationship between the contact points on the rigid-body and express it in terms of velocities. This development is applied in the derivation of an impact law which is used to calculate the impulsive forces associated with impact [13, 19].

Friction at the impacting surface is examined as a complementarity problem and a set of complementarity conditions using Coulomb's friction law are established to address the tangential velocities [7, 20]. This formulation determines the feasible sticking and slipping regions based on the static and dynamic coefficients of friction. These feasible regions have also been known to depend on the angle of impact [12, 21], and will be considered in this work. It has been noted in the literature that a discontinuity arises in the stick-slip transition when using a complementarity formulation [1, 3]. This discontinuity has been addressed by making the transition continuous using a contact stress model [22, 23]. This cannot be applied in this work which considers a rigid-body system. Instead, a Karnopp model is implemented in this work to smooth the transition betweeen the stick and slip regions [8]. Additional constraints are needed to yield a solution for the velocities in the tangential direction [3, 21]. Thus, a dissipation principle is formulated such that a quantity of interest is minimized and converges to a feasible solution. Here, the distance between the known solution and the no-slip solution in the complementarity conditions is minimized as in [12]. As a result, an optimization of the tangential velocity is accomplished and a unique coefficient of friction is found based on the impulsive forces at the impact point. The post-impact velocities can then be computed to simulate the post-impact behavior of the system.

CHAPTER 3

PROBLEM STATEMENT

3.1 Indeterminate Equations

A careful look at the equations of motion where the forces involved due to impact must be considered,

$$A\ \ddot{\mathbf{q}} + \mathbf{b}(\mathbf{q}, \dot{\mathbf{q}}) + \mathbf{g}(\mathbf{q}) = J^T(\mathbf{q})\mathbf{F} + \mathbf{\Gamma} \tag{3.1}$$

where A is the mass matrix and J is a Jacobian matrix that defines the velocity and forces at the impact points. The generalized coordinates are included in $\mathbf{q}$, while $\mathbf{b}$, $\mathbf{g}$, $\mathbf{F}$, and $\mathbf{\Gamma}$ are vectors of velocity, gravity, impact and external forces, respectively.

For the planar system of a rigid ball considered in this work, there are no external forces present on the body. The equations of motion for this system take the form of,

$$\begin{bmatrix} m_A & 0 & 0 \\ 0 & m_A & 0 \\ 0 & 0 & IA_3 \end{bmatrix} \begin{bmatrix} \ddot{Q}_1 \\ \ddot{Q}_2 \\ \ddot{Q}_3 \end{bmatrix} + \begin{bmatrix} 0 \\ m_A\ g \\ 0 \end{bmatrix} = \begin{bmatrix} 1 & 0 & 0 & 1 \\ 0 & 1 & 1 & 0 \\ R & 0 & R & 0 \end{bmatrix} \begin{bmatrix} F_1 \\ F_2 \\ F_3 \\ F_4 \end{bmatrix} \tag{3.2}$$

where m_A is the mass of the body, IA_3 is the moment of inertia, and g is gravity. This gives three equations but four unknowns defined by $F_1, F_2, F_3,$ and F_4. It can be concluded that these equations of motion are indeterminate with respect to the impact forces. A unique method will be introduced in the following section which seeks to overcome this obstacle.

3.2 Velocity Constraint

The theory of rigid-body dynamics will be examined in order to address the problem proposed in Sec. 3.1. In this work, the system being considered is a rigid-body where it is assumed no deformations take place. This assumption defines that the distance between a point on the body will remain the same distance from all the other points on the body [18]. This idea can be extended to examine the relationship of the velocities between different points on a rigid-body. Consider the planar example of a rigid ball illustrated in Fig. 3.1 with angular velocity, $\boldsymbol{\omega}$, and points A, 1, and 2 defined on the body.

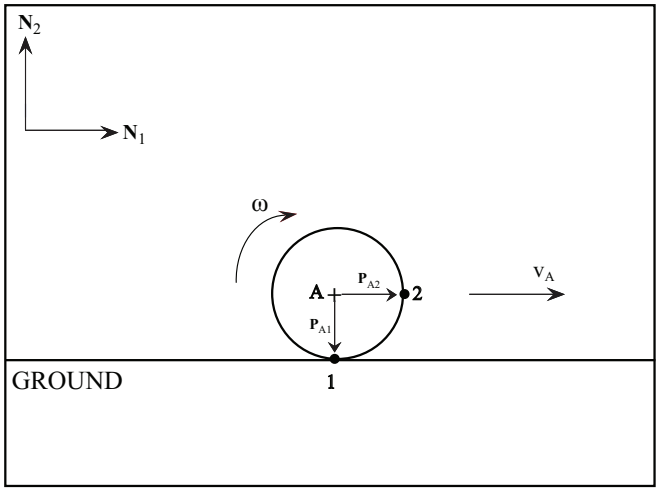

Figure 3.1. Example of Planar Rigid Ball.

If the velocity of ball's center of mass at point A is known, $\mathbf{v_A}$, with respect to an inertial reference frame, shown as $\mathbf{N_1}$ and $\mathbf{N_2}$ in Fig. 3.1, then the velocity of point 1 and 2 can be found by [18],

$$\mathbf{v_1} = \mathbf{v_A} + \mathbf{v_{1/A}} \tag{3.3}$$

and

$$\mathbf{v_2} = \mathbf{v_A} + \mathbf{v_{2/A}} \tag{3.4}$$

where $\mathbf{v_{1/A}}$ is the relative velocity between points 1 and A and $\mathbf{v_{2/A}}$ is the relative velocity between points 2 and A. These velocities can be defined as,

$$\mathbf{v_{1/A}} = \boldsymbol{\omega} \times \mathbf{P_{A1}} \tag{3.5}$$

and

$$\mathbf{v_{2/A}} = \boldsymbol{\omega} \times \mathbf{P_{A2}} \tag{3.6}$$

The quantities $\mathbf{P_{A1}}$ and $\mathbf{P_{A2}}$ shown in Fig. 3.1 are the position vectors from the center of mass to the point of interest. By substituting (3.5) and (3.6) into (3.3) and (3.4), then the complete expression of the velocities at point 1 and 2 can be obtained,

$$\mathbf{v_1} = \mathbf{v_A} + \boldsymbol{\omega} \times \mathbf{P_{A1}} \tag{3.7}$$

and

$$\mathbf{v_2} = \mathbf{v_A} + \boldsymbol{\omega} \times \mathbf{P_{A2}} \tag{3.8}$$

Subtracting (3.7) from (3.8) to eliminate $\mathbf{v_A}$, the relationship for the velocities between point 1 and 2 can be expressed as,

$$\mathbf{v_2} - \mathbf{v_1} = (\boldsymbol{\omega} \times \mathbf{P_{A2}}) - (\boldsymbol{\omega} \times \mathbf{P_{A1}}) \tag{3.9}$$

Finally, by moving $\mathbf{v_1}$ to the right side of (3.9) and combining the cross products, the velocity of point 2 can be expressed as,

$$\mathbf{v_2} = \mathbf{v_1} + \boldsymbol{\omega} \times (\mathbf{P_{A2}} - \mathbf{P_{A1}}) \tag{3.10}$$

A careful look at the result in (3.10), shows that it can be simplified further. Using vector addition,

$$\mathbf{P_{A2}} - \mathbf{P_{A1}} = \mathbf{P_{12}} \tag{3.11}$$

such that (3.10) becomes,

$$\mathbf{v_2} = \mathbf{v_1} + \boldsymbol{\omega} \times \mathbf{P_{12}} \tag{3.12}$$

which provides a clear relationship between the velocities at point 1 and 2.

The result in (3.12) can be used to define the relationship between the velocities at each contact point. The planar model introduced in Sec. 1.1 can be illustrated as in Fig. 3.2, where the velocity of the rigid ball is defined by $\mathbf{v_A}$ and the contact forces have been replaced by normal and tangential velocities at the contact points.

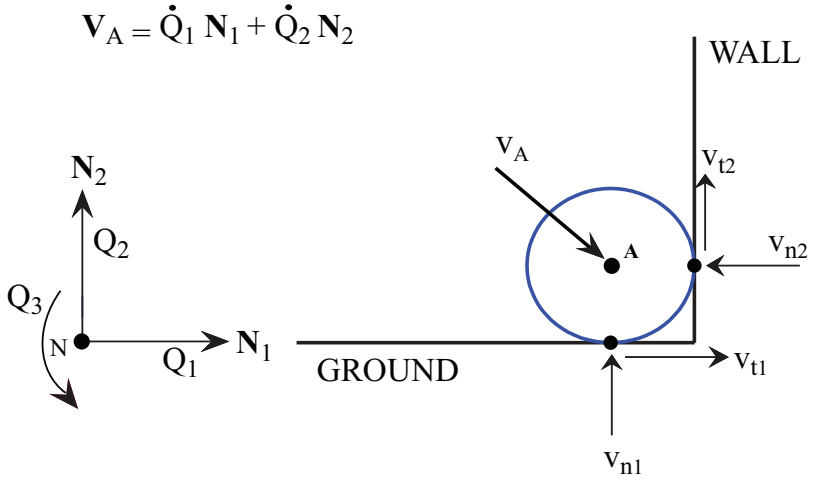

Figure 3.2. Relationship Between Contact Points.

The terms $\mathbf{v_1}$ and $\mathbf{v_2}$ in (3.12) contain the normal and tangential velocities of the contact points at the ground and wall, respectively, such that,

$$\begin{bmatrix} v_{n_2} \\ v_{t_2} \\ 0 \end{bmatrix} = \begin{bmatrix} v_{t_1} \\ v_{n_1} \\ 0 \end{bmatrix} + \begin{bmatrix} 0 \\ 0 \\ \dot{Q}_3 \end{bmatrix} \times \begin{bmatrix} R \\ R \\ 0 \end{bmatrix} \tag{3.13}$$

The subscripts n and t distinguish between normal and tangential velocities and $\boldsymbol{\omega} = \dot{Q}_3 \, \mathbf{N_3}$. The cross product in (3.13) can be carried out to give,

$$\begin{bmatrix} v_{n_2} \\ v_{t_2} \\ 0 \end{bmatrix} = \begin{bmatrix} v_{t_1} \\ v_{n_1} \\ 0 \end{bmatrix} + \begin{bmatrix} -R \, \dot{Q}_3 \\ R \, \dot{Q}_3 \\ 0 \end{bmatrix} \tag{3.14}$$

which gives two expressions in the $\mathbf{N_1}$ and $\mathbf{N_2}$ directions as is expected for the planar system being considered. The first two equations in (3.14) can be summed to produce a relationship among the velocities at the contact points,

$$v_{n_2} + v_{t_2} = v_{t_1} + v_{n_1} \tag{3.15}$$

or

$$v_{n_2} + v_{t_2} - v_{t_1} - v_{n_1} = 0 \tag{3.16}$$

The relation in (3.16) demonstrates the coupling between the velocities at the contact points. Any of the velocities can be defined as a function of the others and thus, a constraint can be formulated. In this way, the rigid-body assumption has allowed for the definition of a constraint which can be applied to the equations of motion to make them determinate. This procedure will be demonstrated in the following section.

3.3 Constraint Implementation

The dual nature of the impact Jacobian expresses the relationship between velocities and forces,

$$\boldsymbol{\vartheta} = \begin{bmatrix} \mathbf{v}_1 \\ \boldsymbol{\omega}_1 \\ \vdots \end{bmatrix} = J \, \dot{\mathbf{q}} \qquad \mathbf{F} = \begin{bmatrix} \mathbf{f}_1 \\ \mathbf{m}_1 \\ \vdots \end{bmatrix} \tag{3.17}$$

where $\mathbf{v}_i$ and $\boldsymbol{\omega}_i$ are the translational and angular velocity of the i^{th} impact point. The $\mathbf{f}_i$ and $\mathbf{m}_i$ terms are the force and moment acting on the body at the i^{th} impact

point. For the planar model of the rigid ball examined in this work, the velocities of the contact points can be expressed in $\boldsymbol{\vartheta}$ as,

$$\boldsymbol{\vartheta} = \begin{bmatrix} v_{t_1} \\ v_{n_1} \\ v_{t_2} \\ v_{n_2} \end{bmatrix} \tag{3.18}$$

where the subscripts t and n denote tangential and normal, respectively. The subscript 1 is for ground contact and 2 is for wall contact.

The velocity constraint obtained in (3.16) will be used to constrain one of the tangential velocities and focus the analysis on the other contact point. Consider an example where the wall contact point is examined and the tangential velocity at the ground, v_{t_1}, is constrained. This is accomplished by expressing v_{t_1} in terms of all the other velocities such that,

$$v_{t_1} = -v_{n_1} + v_{t_2} + v_{n_2} \tag{3.19}$$

Substituting the expression in (3.19) for the first entry in (3.18) gives,

$$\boldsymbol{\vartheta} = \begin{bmatrix} v_{t_1} \\ v_{n_1} \\ v_{t_2} \\ v_{n_2} \end{bmatrix} = \begin{bmatrix} -v_{n_1} + v_{t_2} + v_{n_2} \\ v_{n_1} \\ v_{t_2} \\ v_{n_2} \end{bmatrix} = \begin{bmatrix} -1 & 1 & 1 \\ 1 & 0 & 0 \\ 0 & 1 & 0 \\ 0 & 0 & 1 \end{bmatrix} \begin{bmatrix} v_{n_1} \\ v_{t_2} \\ v_{n_2} \end{bmatrix} \tag{3.20}$$

where the coefficients of v_{n_1}, v_{t_2}, and v_{n_2} have been extracted and put into matrix form. Thus, an expression for the velocities of the impact points and its subset in (3.20) is given by,

$$\boldsymbol{\vartheta} = z^* \, \boldsymbol{\vartheta}^* \tag{3.21}$$

where z^* is a permutation matrix containing the velocity constraint and $\boldsymbol{\vartheta}^*$ contains the remaining velocities. Recall from (3.17) the relationship between the velocities of the impact points and the generalized velocities,

$$\boldsymbol{\vartheta} = J\ \dot{\mathbf{q}} \tag{3.22}$$

A similar expression can be obtained to express the remaining set of velocities and the generalized velocities as,

$$\boldsymbol{\vartheta}^* = J^*\ \dot{\mathbf{q}} \tag{3.23}$$

where J^* is a constrained Jacobian matrix. By substituting (3.22) and (3.23) into (3.21), gives,

$$J\ \dot{\mathbf{q}} = z^*\ J^*\ \dot{\mathbf{q}} \tag{3.24}$$

such that,

$$J\ = z^*\ J^* \tag{3.25}$$

The expression in (3.25) represents the relationship between the original Jacobian and the constrained Jacobian, given by z^*. Based on the dual nature of the Jacobian, an expression can be obtained to represent the constraint in terms of the contact forces by taking the transpose of (3.25),

$$J^T = J^{*T}\ z^{*T} \tag{3.26}$$

Revisiting the equations of motion presented in Sec. 3.1, where there are no velocity terms and external forces, then

$$A\ \ddot{\mathbf{q}} + \mathbf{g}\ (\mathbf{q}) = J^T(\mathbf{q})\ \mathbf{F} \tag{3.27}$$

The result in (3.26) can be substituted in (3.27) to implement the constraint developed to give,

$$A\ \ddot{\mathbf{q}} + \mathbf{g}\ (\mathbf{q}) = J^{*T}(\mathbf{q})\ \mathbf{F}^* \tag{3.28}$$

where

$$\mathbf{F}^* = z^{*T}\ \mathbf{F} \tag{3.29}$$

The term $\mathbf{F}^*$ contains a constrained set of impact forces. Hence, the equations of motion have been converted to become determinate and are represented in (3.28). The difficulty of calculating the impact forces is overcome with the implementation of the constraint which was developed in Sec. 3.2. In the following section, the analysis will be extended to calculate the impulsive forces and evaluate the slip-state at the impact points.

CHAPTER 4

RESOVLING POST-IMPACT VELOCITIES

4.1 Impact Law

The developments made in Sec. 3.3 can be used to calculate the impulsive forces. It is important to know what the impulsive forces are to evaluate the slip-state of each contact point. Using the expression for the equations of motion obtained in (3.28) from Sec. 3.3, a definite integration of the dynamic model over a short time period ϵ yields,

$$\int_t^{t+\epsilon} (A\ \ddot{\mathbf{q}} + \mathbf{g}\ (\mathbf{q}))\ dt = \int_t^{t+\epsilon} J^{*T}(\mathbf{q})\ \mathbf{F}^*\ dt \tag{4.1}$$

which gives,

$$A\ (\ \dot{\mathbf{q}}(t+\epsilon) - \dot{\mathbf{q}}(t)\ ) = J^{*T}\ \mathbf{p}^* \tag{4.2}$$

Multiplying both sides by the inverse of the mass matrix gives,

$$\dot{\mathbf{q}}(t+\epsilon) - \dot{\mathbf{q}}(t) = A^{-1}\ J^{*T}\ \mathbf{p}^* \tag{4.3}$$

in which m $\leq$ n making it an underconstrained system of equations. The two unknowns in (4.3) are $\dot{\mathbf{q}}(t+\epsilon)$ and $\mathbf{p}^*$. Not all of the terms in $\dot{\mathbf{q}}$ contribute to the impact forces contained in $\mathbf{p}^*$. Recall the expression obtained in (3.23),

$$\boldsymbol{\vartheta}^* = J^*\ \dot{\mathbf{q}} \tag{4.4}$$

Thus, the contributing terms in $\dot{\mathbf{q}}$ can be expressed as the velocities of the impact points with the use of (4.4),

$$\boldsymbol{\vartheta}^*(t+\epsilon) - \boldsymbol{\vartheta}^*(t) = J^*\ A^{-1}\ J^{*T}\mathbf{p}^* \tag{4.5}$$

resulting in a one-to-one mapping between the velocities and forces involved at impact. Solving for $\mathbf{p}^*$ gives,

$$\left(J^* A^{-1} J^{*T}\right)^{-1} \left(\boldsymbol{\vartheta}^*(t+\epsilon) - \boldsymbol{\vartheta}^*(t)\right) = \mathbf{p}^* \tag{4.6}$$

The impulsive forces for all the contact points can then be obtained by removing the constraint previously used by,

$$\mathbf{p} = z^T \mathbf{p}^* \tag{4.7}$$

where,

$$z^T = \left[\left(z^{*T}\ z^*\right)^{-1}\ z^{*T}\right]^T \tag{4.8}$$

Thus, the impact law can be stated as,

$$\mathbf{p} = z^T\ \left(J^* A^{-1} J^{*T}\right)^{-1} \left(\boldsymbol{\vartheta}^*(t+\epsilon) - \boldsymbol{\vartheta}^*(t)\right) \tag{4.9}$$

Using the formulation demonstrated above, it is possible to calculate all the impulsive forces at impact. The difficulty of dealing with equations of motion which are indeterminate is overcome with the application of a velocity constraint based on the rigid-body assumption. This approach will be used herein to calculate the impulsive forces and provide a basis for determining the slip-state of each contact point.

4.2 Complementarity Conditions

In this work, friction is treated as a complementarity problem. The complementarity formulation defines the range of values for velocities, accelerations, and forces at the impact points. For the case in the normal direction, the velocity of the impact point undergoes a change in direction as it approaches zero. Thus, the acceleration

must be checked to ensure that contact was made given by the second expression in (4.10).

$$\begin{cases} v_{n_i}(t) < 0 & \text{impact or contact} \\ v_{n_i}(t) = 0 \quad \text{and} & \begin{cases} \dot{v}_{n_i}(t) \leq 0 \text{ contact} \\ \dot{v}_{n_i}(t) > 0 \text{ separation} \end{cases} \\ v_{n_i}(t) > 0 & \text{separation} \end{cases} \tag{4.10}$$

After contact has been detected, the post-impact velocity in the normal direction is simply determined with the use of Newton's COR which is a function of the normal velocity before impact. Hence, the post-impact normal velocity takes the form of,

$$v_{n_i}(t+\epsilon) = -e_{n_i} v_{n_i}(t) \tag{4.11}$$

such that $0 \leq e_{n_i} \leq 1$ and $e_{n_i} \neq 0$ is used to model rebound.

The use of Coulomb's friction law establishes a set of complementarity conditions for the tangential velocity at the impact point. The post-impact velocity must satisfy,

$$\begin{cases} v_{t_i} = 0 \text{ and } \dot{v}_{t_i} = 0 & \text{then} \quad \|\mathbf{f}_{t_i}\| \leq \mu_s \, |\mathrm{f}_{n_i}| \\ v_{t_i} = 0 \text{ and } \dot{v}_{t_i} \neq 0 & \text{then} \quad \|\mathbf{f}_{t_i}\| = \mu_s \, |\mathrm{f}_{n_i}| \\ v_{t_i} \neq 0 & \text{then} \quad \|\mathbf{f}_{t_i}\| = \mu_d \, |\mathrm{f}_{n_i}| \end{cases} \tag{4.12}$$

where the first relation is the no-slip condition, the second describes the stick-slip transition, and the last relation defines slipping.

The static, μ_s, and dynamic, μ_d, coefficients of friction used in (4.12) define the regions for sticking and slipping in the tangential direction. The boundary between sticking and slipping can be visualized by a friction cone as in Fig. 4.1.

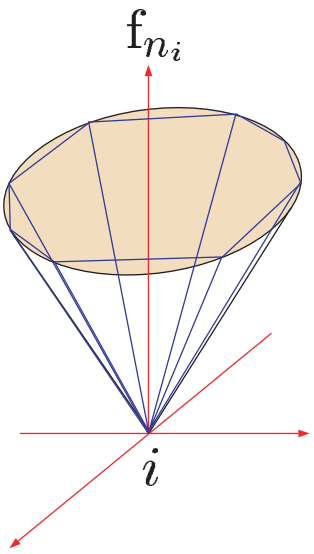

Figure 4.1. Friction Cone.

Past work has also discovered that the angle of impact has an effect on the feasible regions for sticking and slipping [12, 21]. This will be considered in this work by varying the angle of impact for the system. It is important to note the transition region which exists between sticking and slipping which is known as the stick-slip boundary. This boundary presents a discontinuity when determining the slip-state of each contact point. This discontinuity cannot be eliminated but only be attenuated. In this work, a Karnopp model is implemented which helps smooth the transition between the sticking and slipping regions [8].

The complementarity conditions (4.12) can also be represented in terms of impulses as in [9],

$$\begin{cases} v_{t_i} = 0 \text{ and } \dot{v}_{t_i} = 0 & \text{then} \quad \|\mathbf{p}_{t_i}\| \leq \mu_s \, |\mathrm{p}_{n_i}| \\ v_{t_i} = 0 \text{ and } \dot{v}_{t_i} \neq 0 & \text{then} \quad \|\mathbf{p}_{t_i}\| = \mu_s \, |\mathrm{p}_{n_i}| \\ v_{t_i} \neq 0 & \text{then} \quad \|\mathbf{p}_{t_i}\| = \mu_d \, |\mathrm{p}_{n_i}| \end{cases} \tag{4.13}$$

Similarly, the first relation defines the no-slip condition, the second expression is the stick-slip transition, and the third defines slipping. The tangential velocities are

initially assumed to be zero and the impulsive forces are calculated at each contact point to check the no-slip condition. If the no-slip condition is violated, then it will be clear that the contact point is slipping such that none of the tangential COR's are known. Any assumptions made about the state of the contact point would be incorrect because of the simultaneous solution obtained from the system of equations.

Only the feasible regions are for sticking and slipping have been defined thus far. A unique solution exists for the case when all the contact points stick. In order to obtain a solution when at least one of the contact points slip, then additional constraints are needed which will be discussed in the following section.

4.3 Dissipation Principle

The developments made in Sec. 4.2 only define the feasible range of values for velocities, accelerations, and forces at the contact points. In order to resolve the post-impact velocities when slip occurs, then additional constraints are needed. A dissipation principle is formulated which utilizes the no-slip condition presented in the complementarity conditions. This condition which is the first relation in (4.13) has been modified to be,

$$\frac{\|\mathbf{p}_{t_i}\|}{|\mathrm{p}_{n_i}|} \;\geq\; \mu_i(\boldsymbol{\vartheta}(t+\epsilon)) \tag{4.14}$$

where the static coefficient of friction has been replaced by a general one, and

$$\begin{cases} 0 \;\leq\; \mathrm{p}_{n_i} & \text{ground contact} \\ \\ 0 \;\geq\; \mathrm{p}_{n_i} & \text{wall contact} \end{cases} \tag{4.15}$$

for $i \in \{1, \ldots, m\}$. The condition in (4.15) ensures that the impacting point does not penetrate the surface. The μ_i obtained in (4.14) is uniquely calculated by $\mathbf{p}_{t_i}$ and p_{n_i} which are functions of $\boldsymbol{\vartheta}(t+\epsilon)$.

The dissipation principle used in this work considers the coefficients of friction and restitution and determines their feasibility. If these coefficients are found to be infeasible, then the dissipation principle ensures a feasible μ is achieved. This is accomplished by minimizing the distance from the known solution to the no-slip solution defined as,

$$\mathbf{d} \;=\; \begin{bmatrix} \mu_s \\ 0 \end{bmatrix} - \begin{bmatrix} \mu_i \\ v_{t_i}(t+\epsilon) \end{bmatrix} \tag{4.16}$$

subject to a complementarity condition which allows expressions for the nonconvex feasible region as,

$$\min_{\left(v_{t_i}(t+\epsilon)\right)} \qquad \text{obj} \;:=\; \mathbf{d}^T\,\mathbf{d} \tag{4.17}$$

subject to

$$\mathbf{p}_{t_i}^T\,\mathbf{p}_{t_i} - \mu_i^2\;\mathrm{p}_{n_i}^2 \;\geq\; 0 \tag{4.18}$$

$$\begin{cases} 0 \;\leq\; \mathrm{p}_{n_i} & \text{ground contact} \\ \\ 0 \;\geq\; \mathrm{p}_{n_i} & \text{wall contact} \end{cases} \tag{4.19}$$

where,

$$z^T\;\left(J^* A^{-1} J^{*T}\right)^{-1}\left(\boldsymbol{\vartheta}^*(t+\epsilon) - \boldsymbol{\vartheta}^*(t)\right) = \;\mathbf{p} \tag{4.20}$$

$$\min\left(\mu_d,\;\mu_{f_i}\right) \;=\; \mu_{min_i} \tag{4.21}$$

$$\mu_{min_i} \;+\; \left(\mu_s - \mu_{min_i}\right)\;\mathrm{e}^{-\left(\frac{\|v_{t_i}\|}{v_s}\right)^a} \;=\; \mu_i \tag{4.22}$$

for $i \in \{1, \ldots, m\}$. The objective function used here performs like a maximum dissipation principle by minimizing the value of the tangential velocity. The decision variables used in the optimization are contained within (4.17). The constraint in

(4.18) has been modified and represents the no-slip condition from the complementarity conditions in (4.13). The constraints shown in (4.19) ensure the contact point does not penetrate the contacting surface. The relation in (4.20) shows how the impulsive forces are calculated according to the impact law developed in Sec. 4.1. The constraint in (4.21) ensures the smaller quantity between μ_d and μ_{f_i} is used in the Karnopp model in (4.22). The value of μ_{f_i} corresponds to the coefficient of friction when $v_{t_i} = 0$. For this work, $v_s = 1.4 \times 10^{-4} m/s$ and a = 1 such that when $\|v_{t_i}\| \approx 1 \times 10^{-3},\ \mu_i \approx \mu_{min}$. Similarly, when $\|v_{t_i}\| \approx 0,\ \mu_i \approx \mu_s$. In this way, the discontinuity in the stick-slip transition is addressed.

Using this formulation, the feasible post-impact tangential velocity of the contact point can be resolved. The feasible solution for the tangential velocity at the other contact point is calculated using the velocity constraint. This solves for all the post-impact velocities which are used as the initial conditions before restarting the simulation. A depiction of the post-impact dynamic behavior can be realized and three cases considered will be presented in the following section.

CHAPTER 5

SIMULATION RESULTS

In the following cases considered, the coefficient of restitution is 0.5 and the value of μ_s and μ_d are 0.5 and 0.25, respectively. The results of three cases are presented.

5.1 Case 1: Angle of impact, $\theta \approx 60^\circ$

In the first case examined, the ball impacts the corner at approximately 60° with respect to the ground. The initial parameters are listed in Table 5.1 for this case.

Table 5.1. Case 1: Initial Parameters

Position	Q_1	Q_2	Q_3
	0 m	5 m	0 rad
Velocity	$\dot{Q}_1$	$\dot{Q}_2$	$\dot{Q}_3$
	4 m/s	0 m/s	0 rad/s

The no-slip condition in (4.13) was used to check for slip after calculating the impulsive forces and the result indicated that the contact points were slipping. For this case, the wall contact point is examined based on the steep angle of impact and the constraint is enforced on the tangential velocity at the ground. By finding a feasible tangential velocity at the wall, then the velocity constraint in (3.16) can be used to determine the soluton for the tangential velocity at the ground.

It is necessary to determine what feasible values for the tangential velocity at

the wall lie in the stick region, if any exist, or in the region for slipping. The μ vs. v_t plot shown in Fig. 5.1 was used to depict the location of these feasible regions. The curve represents the constraint in (4.18) when it is equal to zero and the region below the curve satisfies this constraint. The dotted line across the plot is μ_f and defines the value of μ when the curve crosses the $v_t = 0$ line. The line which extends from the intersection of the curve and μ_f down to the value of μ_s defines the feasible stick region. Lastly, the shaded region on the left side of the plot is infeasible and is imposed by the constraint in (4.19) for wall contact.

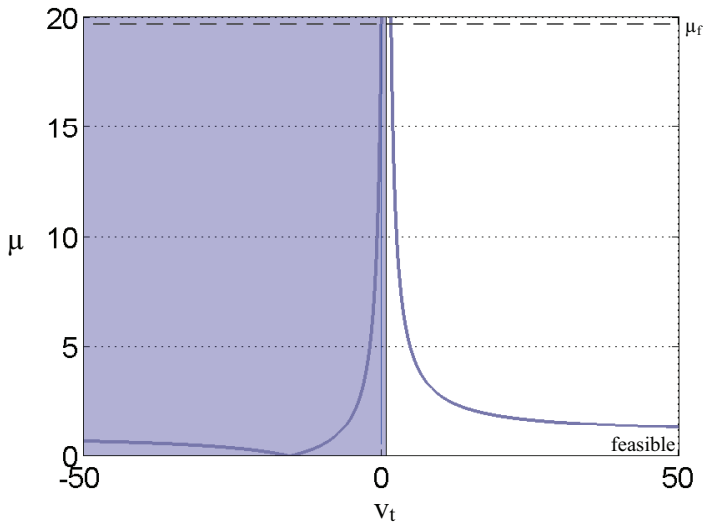

Figure 5.1. Case 1: μ vs. v_t for $e = 0.5$.

The results from this plot can be interpreted to indicate that since $v_t = 0$ lies in the infeasible region, then the wall contact point must slip. The tangential velocity can only approach but never be zero. Hence, the region below the curve and to the right of the infeasible region defines the feasible slip region and the range of feasible tangential velocities. The optimization was started in this feasible region to obtain the minimum tangential velocity at the wall. The post-impact normal velocities were

then resolved using Newton's COR and the tangential velocity at the ground was calculated using the velocity constraint developed in this work. The simulation was then restarted with these velocities serving as the initial conditions.

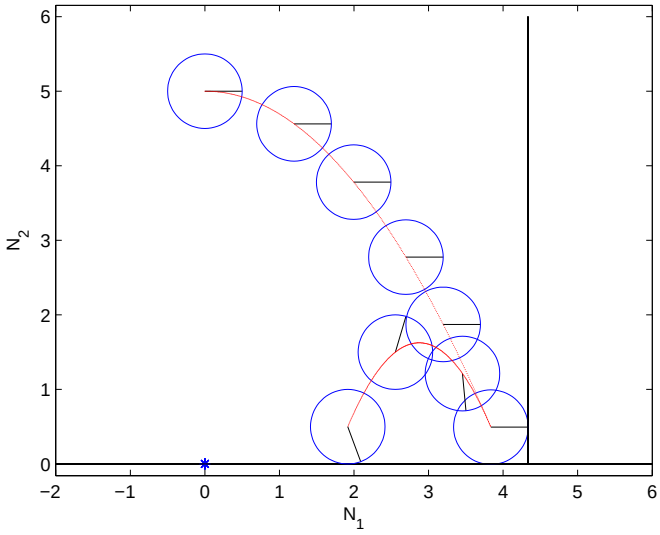

Figure 5.2. Simulation Results for Case 1.

The overall simulation of the ball for Case 1 is illustrated in Fig. 5.2. The curve in the figure depicts the translation of the ball's mass center throughout the simulation, before and after impact. The ball obtains a negative angular rotation after impact which is consistent with the fact that the contact points slip as result of the impact.

It was also useful to examine the total energy of the system during the impact event to ensure there were no energy gains. In Fig. 5.3, the potential, kinetic, and total energy of the system are plotted throughout the simulation. The total energy of the system decreased with no uncharacteristic energy gains, which was consistent with what was expected for an impact.

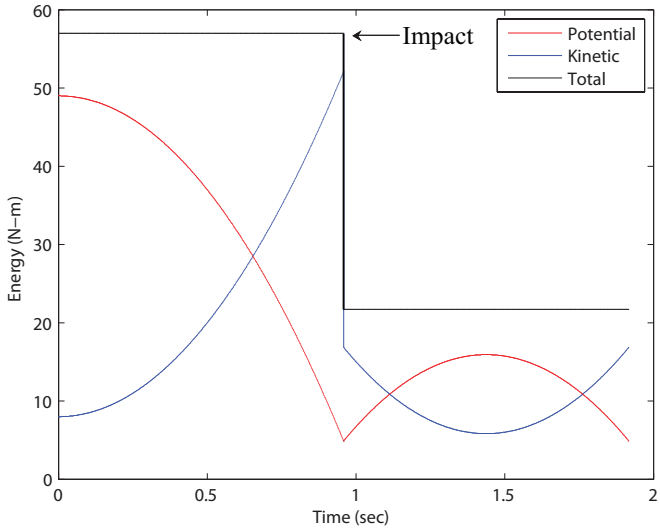

Figure 5.3. Energy Consistency for Case 1.

5.2 Case 2: Angle of impact, $\theta \approx 30°$

The second case considered in this work, examined the ball impacting the corner at approximately 30° with respect to the ground. The initial paramters used for this case are listed in Table 5.2.

Table 5.2. Case 2: Initial Parameters

Position	Q_1	Q_2	Q_3
	0 m	1.5 m	0 rad
Velocity	$\dot{Q}_1$	$\dot{Q}_2$	$\dot{Q}_3$
	8 m/s	0 m/s	0 rad/s

The impulsive forces were calculated to check the no-slip condition and it was found that the contact points were slipping. Unlike the approach taken in Case 1, the ground contact point was examined to find a feasible solution, while the tangential velocity at the wall was constrained. The μ vs. v_t plot shown in Fig. 5.4 was then used to locate the feasible sticking and slipping regions.

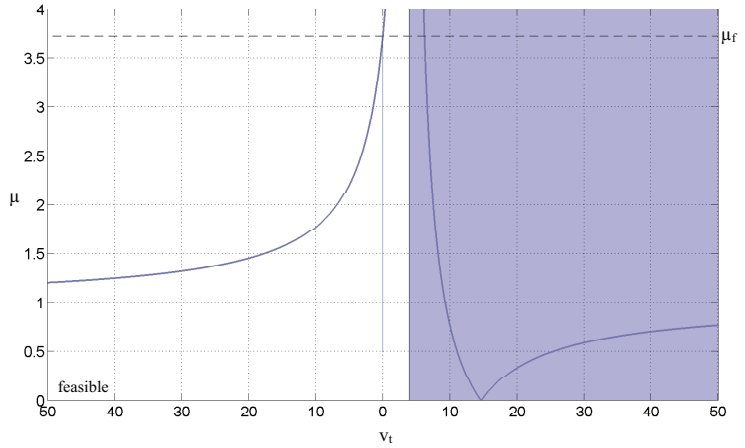

Figure 5.4. Case 2: μ vs. v_t for $e = 0.5$.

The constraints depicted in the plot are similar to Fig. 5.1 observed in Case 1, except for the shaded region imposed by the impenetrability constraint. In this case, it is on the right side of the plot since the constraint in (4.19) for ground contact was being considered. From Fig. 5.4, it was concluded that a feasible solution for sticking existed because $v_t = 0$ lies in the feasible region. This region is below the curve defined by the constraint in (4.18) and to the left of the infeasible region imposed by the normal impulsive force. Hence, the optimization was started in this feasible region and the tangential velocity at the ground was minimized to approach $v_t = 0$.

The post-impact normal velocities were resolved using Newton's COR and the tangential velocity at the wall was calculated using the velocity constraint. These velocities served as the initial conditions when the simulation was restarted. The result of the overall simulation for Case 2 is illustrated in Fig. 5.5.

The curve in the figure represents the translation of the ball's mass center throughout the simulation. Since a feasible stick solution for the tangential velocity at the ground was achieved, the angular velocity of the ball was positive after impacting the corner.

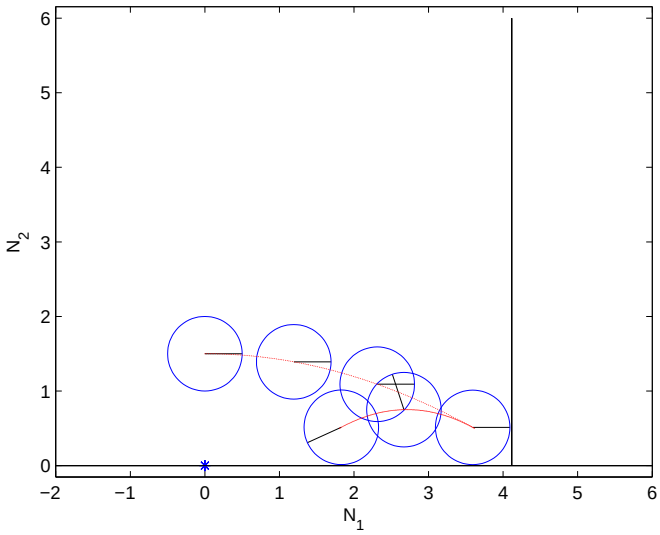

Figure 5.5. Simulation Results for Case 2.

The total energy of the system for this case was also examined and is plotted in Fig. 5.6. The total energy decreased and there were no energy gains as a result of the impact. The plot results were consistent with what was expected for impact.

5.3 Case 3: Angle of impact, $\theta \approx 45°$

The final case considered in this work, examined the ball impacting the corner at approximately 45° with respect to the ground. The initial conditions used for this case are listed in Table 5.3.

Table 5.3. Case 3: Initial Parameters

Position	Q_1	Q_2	Q_3
	0 m	1.5 m	0 rad
Velocity	$\dot{Q}_1$	$\dot{Q}_2$	$\dot{Q}_3$
	4 m/s	0 m/s	0 rad/s

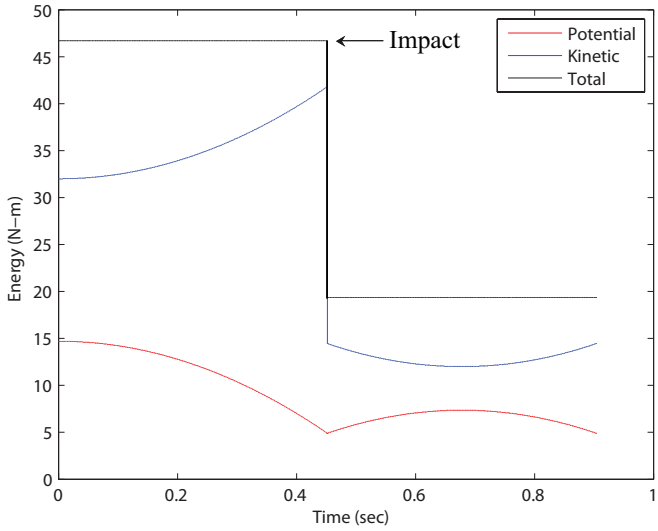

Figure 5.6. Energy Consistency for Case 2.

This case was unique in the sense that it was approached using two different methods. The methods used in Case 1 and 2 were applied, in which the tangential velocity at the ground and wall were constrained independently, and the solutions were compared. The plot of μ vs. v_t for the method used in Case 1, where the tangential velocity at the ground was constrained is shown in Fig. 5.7.

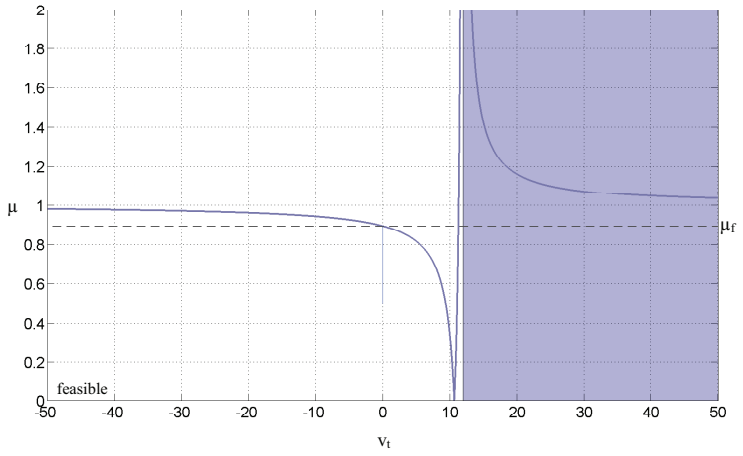

Figure 5.7. Case 3: μ vs. v_t for $e = 0.5$ for wall contact.

For this method, the plot depicted a feasible stick solution since the tangential velocity at the wall can approach the $v_t = 0$ line. The optimization was started in this feasible region to obtain the feasible tangential velocity at the wall. Then, the tangential velocity at the ground was calculated using the velocity constraint and Newton's COR was used for the normal velocities to obtain all the post-impact velocities before restarting the simulation. The results of the simulation are shown in Fig. 5.8 for Case 3 when the tangential velocity at the ground was constrained.

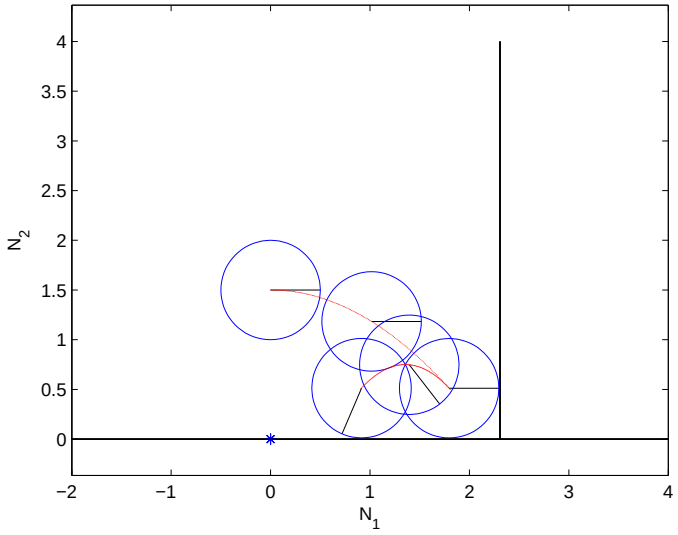

Figure 5.8. Simulation Results for Case 3: v_{t_1} at ground is constrained.

Based on the method used for Case 1, the ball leaves the corner after impact with a negative angular velocity. This was consistent with the fact that the wall contact point sticks, while the contact point at the ground slips. The total energy of the system for this case was plotted throughout the simulation and is shown in Fig. 5.9. The plot illustrates there was a significant amount of energy loss due to the impact at the corner with no energy gains.

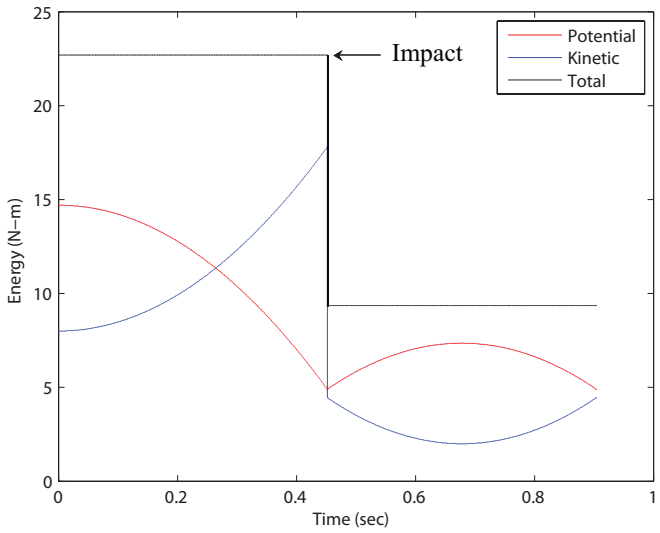

Figure 5.9. Energy Consistency for Case 3: v_{t_1} at ground is constrained.

Next, the method used in Case 2 was applied to analyze this case. For this method, the tangential velocity at the wall was constrained and the ground contact point was examined. The μ vs. v_t plot shown in Fig. 5.10 depicts the feasible regions for sticking and slipping.

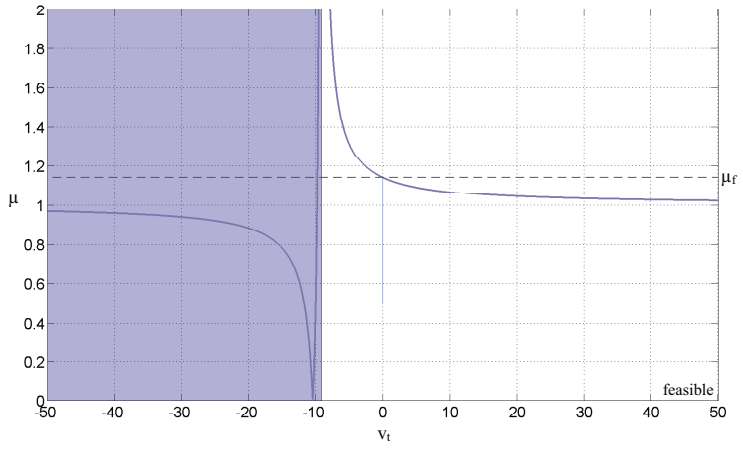

Figure 5.10. Case 3: μ vs. v_t for $e = 0.5$ for ground contact.

It was apparent from the plot that the region for sticking at the ground was attainable for this method as well. The tangential velocity can approach $v_t = 0$ which motivated a solution for sticking at the ground. The same procedure was followed to optimize the tangential velocity at the ground. The post-impact velocities were then resolved and used as the initial conditions for restarting the simulation.

The result of the simulation for Case 3 when the tangential velocity at the wall was constrained is illustrated in Fig. 5.11. The simulation depicted the ball leaving the corner with a positive angular velocity given that the ground contact point sticks. The results from using this method were inconsistent with the results obtained from the first method used. The first method simulated the ball with a negative angular rotation, while the second method resulted in a positive angular rotation. It was concluded that the two simulations were feasible solutions but that neither one was unique. Thus, the application of the method developed in this work allow for the determination of two feasible solutions which serve as reliable approximations for the post-impact behavior of the system.

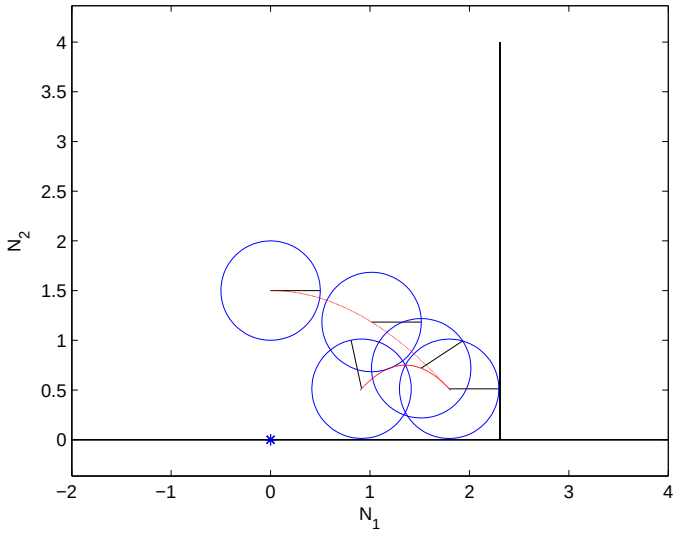

Figure 5.11. Simulation Results for Case 3: v_{t_2} at wall is constrained.

For completeness, the total energy of the ball was examined for this method which is shown in Fig. 5.12. The system remained energetically consistent throughout the impact event. The ball lost a significant amount of its total energy at impact with no energy gains.

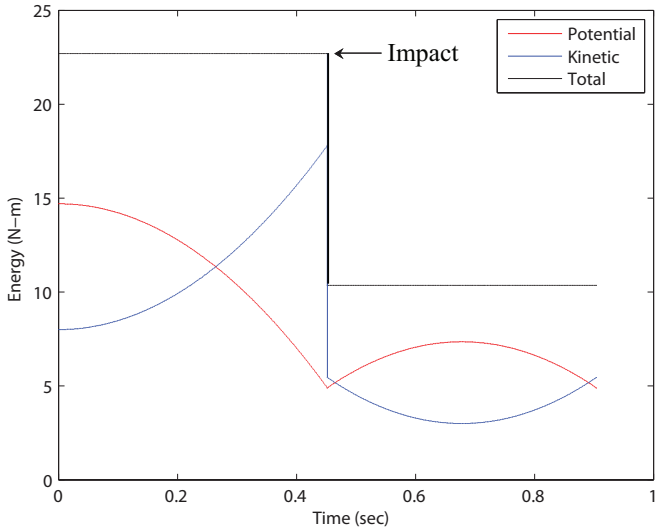

Figure 5.12. Energy Consistency for Case 3: v_{t_2} at wall is constrained.

CHAPTER 6

CONCLUSIONS

In this work, the post-impact behavior of a ball in simultaneous, multi-point contact with friction was examined. The equations of motion of the system were indeterminate with respect to the impact forces. A velocity constraint based on the rigid-body assumption was developed and applied to the equations to make them determinate. The derivation of an impact law was formulated to calculate the impulsive forces, allowing for the slip-state of each contact point to be evaluated. Friction was treated as a complementarity problem and a set of complementarity conditions using Coulomb's friction law were established to treat the velocities in the tangential direction when slip occurs. A Karnopp model was adopted to smooth the discontinuity encountered in the stick-slip transition when determining sticking or slipping. Finally, an objective function was formulated to perform like a maximum dissipation principle which minimized the distance from the known solution to the no-slip solution and considered the coefficients of friction and restitution and evaluated their feasibility. In this way, the post-impact velocities were resolved and the dynamic behavior of the ball was simulated. The results of three cases of a ball impacting a corner at multiple contact points with friction were presented. It was concluded that the developments made in this work give solutions which are not unique but provide two feasible solutions that approximate the post-impact behavior of the system.

APPENDIX A

OVERVIEW OF NUMERICAL INTEGRATION

A.1 Overview of Numerical Integration

The simulation of rigid-body impacts requires a numerical integration of the equations of motion which describe the system,

$$A\ \ddot{\mathbf{q}} + \mathbf{b}(\mathbf{q}, \dot{\mathbf{q}}) + \mathbf{g}(\mathbf{q}) = J^T(\mathbf{q})\mathbf{F} + \mathbf{\Gamma} \tag{A.1}$$

Revisiting the characteristics of a discrete algebraic model described in Sec. 2, the simulation must be stopped at the time of impact. The post-impact velocities are then resolved algebraically before restarting the simulation, in which the updated velocities will serve as an inital condition.

Consider numerically integrating (A.1) by first converting it into two first order differerential equations,

$$\dot{\mathbf{q}} = \mathbf{u} \qquad\qquad \ddot{\mathbf{q}} = \dot{\mathbf{u}} \tag{A.2}$$

such that

$$\mathbf{x} = \begin{bmatrix} \mathbf{q} \\ \mathbf{u} \end{bmatrix} = \int_{\Delta t} \dot{\mathbf{x}}\ dt \tag{A.3}$$

$$\dot{\mathbf{x}} = \begin{bmatrix} \dot{\mathbf{q}} \\ \dot{\mathbf{u}} \end{bmatrix} = \begin{bmatrix} \mathbf{u} \\ A^{-1}(J^T\mathbf{F} + \mathbf{\Gamma} - \mathbf{b} - \mathbf{g}) \end{bmatrix} \tag{A.4}$$

Using an Euler numerical integration of $\dot{\mathbf{x}}$

$$\begin{bmatrix} \mathbf{q}(t_1) \\ \mathbf{u}(t_1) \\ \dot{\mathbf{q}}(t_1) \\ \dot{\mathbf{u}}(t_1) \end{bmatrix} = \begin{bmatrix} \mathbf{q}(t_0) + \Delta t\ \mathbf{u}(t_0) \\ \mathbf{u}(t_0) + \Delta t\ \dot{\mathbf{u}}(t_0) \\ \mathbf{u}(t_1) \\ ... \end{bmatrix} \tag{A.5}$$

and at time t_2

$$\begin{bmatrix} \mathbf{q}(t_2) \\ \mathbf{u}(t_2) \\ \dot{\mathbf{q}}(t_2) \\ \dot{\mathbf{u}}(t_2) \end{bmatrix} = \begin{bmatrix} \mathbf{q}(t_1) + \Delta t\ \mathbf{u}(t_1) \\ \mathbf{u}(t_1) + \Delta t\ \dot{\mathbf{u}}(t_1) \\ \mathbf{u}(t_2) \\ ... \end{bmatrix} \tag{A.6}$$

It is assumed that at time t_0 the two points impact, stick, and do not rebound such that for all $i > 0$, $\mathbf{q}(t_i) = \mathbf{q}(t_0)$. This implies that $\dot{\mathbf{q}}(t_0) = \mathbf{u}(t_0) = 0$.

REFERENCES

[1] Y.-T. Wang, V. Kumar, and J. Abel, "Dynamics of rigid bodies undergoing multiple frictional contacts," *Proceedings-IEEE International Conference on Robotics and Automation*, vol. 3, pp. 2764–2769, May 1992.

[2] L. Johansson, "A linear complementarity algorithm for rigid body impact with friction," *European Journal of Mechanics, A/Solids*, vol. 18, no. 4, pp. 703–717, July 1999.

[3] D. E. Stewart, "Rigid-body dynamics with friction and impact," *SIAM Review*, vol. 42, no. 1, pp. 3–39, Mar. 2000.

[4] L. Johansson, "A newton method for rigid body frictional impact with multiple simultaneous impact points," *Computer Methods in Applied Mechanics Engineering*, vol. 191, pp. 239–254, Nov. 2001.

[5] Y. Maeda, K. Oda, and S. Makita, "Analysis of indeterminate contact forces in robotic grasping and contact tasks," *IEEE International Conference on Intelligent Robots and Systems*, pp. 1570–1575, Oct. 2007.

[6] T. Omata and K. Nagata, "Rigid body analysis of the indeterminate grasp force in power grasps," *IEEE Transactions on Robotics and Automation*, vol. 16, no. 1, pp. 46–54, Feb. 2000.

[7] L. Johansson and A. Klarbring, "Study of frictional impact using a nonsmooth equations solver," *Journal of Applied Mechanics*, vol. 67, no. 2, pp. 267–273, June 2000.

[8] D. Karnopp, "Computer simulation of stick-slip friction in mechanical dynamic systems," *Journal of Dynamic Systems, Measurement and Control, Transactions of the ASME*, vol. 107, no. 1, pp. 100–103, Mar. 1985.

[9] I. Han and B. Gilmore, "Multi-body impact motion with friction-analysis, simulatioin, and experimental validation," *Journal of Mechanical Design, Transactions of the ASME*, vol. 115, no. 3, pp. 412–422, Sept. 1993.

[10] J. Moreau, "Numerical aspects of the sweeping process," *Computer Methods in Applied Mechanics and Engineering*, vol. 177, no. 3, pp. 329–349, May 1999.

[11] B. Brogliato, A. Ten Dam, L. Paoli, F. Génot, and M. Abadie, "Numerical simulation of finite dimensional multibody nonsmooth mechanical systems," *Applied Mechanics Reviews*, vol. 55, no. 2, pp. 107–149, Mar. 2002.

[12] D. M. Flickinger and A. Bowling, "Simultaneous oblique impacts and contacts in multibody systems with friction," *Multibody System Dynamics*, vol. 23, no. 3, pp. 249–261, Mar. 2010.

[13] G. Gilardi and I. Sharf, "Literature survey of contact dynamics modelling," *Mechanism and Machine Theory*, vol. 37, no. 10, pp. 1213–1239, Oct. 2002.

[14] W. Son, "Hybrid dynamic simulation of rigid-body contact with coulomb friction," *IEEE International Conference on Robotics and Automation*, vol. 2, pp. 1376–1381, May 2001.

[15] A. Bowling, D. M. Flickinger, and S. Harmeyer, "Energetically consistent simulation of simultaneous impacts and contacts in multibody systems with friction," *Multibody System Dynamics*, vol. 22, no. 1, pp. 27–45, Aug. 2009.

[16] R. M. Brach, "Formulation of rigid body impact problems using generalized coefficients," *International Journal of Engineering Science*, vol. 36, no. 1, pp. 61–71, Jan. 1998.

[17] H. M. Lankarani and M. F. Pereira, "Treatment of impact with friction in planar multibody mechanical systems," *Multibody System Dynamics*, vol. 6, no. 3, pp. 203–227, Jan. 2001.

[18] A. Bedford and W. Fowler, *Engineering Mechanics: Dynamics*. Pearson Education, Inc., 2008.

[19] S. Djerassi, "Collision with friction; part b: Poisson's and stornge's hypotheses," *Multibody System Dynamics*, vol. 21, no. 1, pp. 55–70, Feb. 2009.

[20] C. Glocker and C. Studer, "Formulation and preparation for numerical evaluation of linear complementarity systems in dynamics," *Multibody System Dynamics*, vol. 13, no. 4, pp. 447–463, May 2005.

[21] T. Liu, "Non-jamming conditions in multi-contact rigid-body dynamics," *Multibody System Dynamics*, vol. 22, no. 3, pp. 269–295, Oct. 2009.

[22] B. Volker, T. Schwager, and T. P$\acute{}$oshcel, "Coefficient of tangential restitution for the linear dashpot model," *Statistical, Nonlinear, and Soft Matter Physics*, vol. 77, no. 1, pp. 011 304–1–12, Jan. 2008.

[23] J. Moreau, "Numerical treatment of contact and friction: the contact dynamics method," *Engineering Systems Design and Analysis*, vol. 76, no. 4, pp. 201–208, July 1996.

BIOGRAPHICAL STATEMENT

Adrian Rodriguez was born in Eagle Pass, Texas in 1987. He received his B.S. degree from The University of Texas at Austin in 2009 in Mechanical Engineering. He was the Teaching Assistant for Measurements II Laboratory in Spring 2010 and Introduction to Robotics in Fall 2010. His current research interest is in the area of robotics with a focus on dynamics. He is also an active member and officer of an honor society and volunteer organization.